SINGLE-CAMERA HIGH-SPEED DIGITAL IMAGE CORRELATION FOR COMPRESSIVE FAILURE ANALYSIS OF COMPOSITE PANELS

Dondish, A.[1], Li, L.[2], Melenka, G.W.[1]*
[1] Department of Mechanical Engineering, Lassonde School of Engineering, York University, North York, Canada
[2] Aerospace Research Centre, National Research Council of Canada, Ottawa, Canada
* Corresponding author (gmelenka@yorku.ca)

Abstract

High-speed full-field measurement techniques are an effective tool for fracture analysis of advanced materials such as carbon fibre reinforced polymers (CFRP). For high-speed three-dimensional digital image correlation (3D DIC), the high cost of high-speed cameras motivated the development of strategies for 3D deformation and strain measurement using a single high-speed camera. This work investigates the failure behaviour of CFRP panels in compression after impact (CAI) testing, using a single-camera 3D DIC technique with a four-mirror optical configuration that allows for imaging of two different angular views of a sample within the same camera field of view. This work focuses on a case with 75 Joule (J) of impact energy and is part of a larger study conducted for a variety of impact energy levels. Out-of-plane displacement measurements demonstrated the onset of local buckling and the crack propagation across the width of the testing panels throughout the fracture event. Axial strain measurements demonstrated the compressive strain where local buckling was present and the strain relaxation where the surrounding regions experienced elastic recovery. Comparison of results with those from conventional twin-camera 3D DIC demonstrated a significant cost benefit of the single-camera system, as it costs roughly 54% of an equivalent twin-camera system.

Keywords*: three-dimensional digital image correlation, compressive fracture, high-speed imaging*

1 Introduction

Composite materials are used in lightweight structures in the aerospace and automotive industries for their high strength-to-weight ratio. A critical design consideration in the development of composite structures for aerospace applications is their mechanical response under dynamic loads, such as fracture progression behaviour. A commonly used fibre reinforced composite material is carbon fibre reinforced polymers (CFRP), which provide higher specific strength and stiffness. However, CFRP structures have unfavourable toughness characteristics, resulting in brittle fracture behaviours [1]. These fracture events, which occur over very short time periods, require high-speed measurement techniques for appropriate characterization.

For an investigation of fracture events, high-speed full-field measurement techniques are a powerful tool to map the distributions of deformation and strain over a full field of a test sample surface. Optical full-field measurement techniques for an investigation of fracture events include high-speed digital image correlation (DIC), used in works by Wan et al. [2] and Pan et al. [3], and high-speed infrared thermography (IRT), used in works by Lisle et al. [4] and Yuan et al. [5]. High-speed three-dimensional digital image correlation (3D DIC) is used to measure in-plane and out-of-plane deformations and strains and typically uses a system of two high-speed cameras. This technique was used in the investigation of failure mechanisms of CFRP laminates under compression after impact (CAI) testing [6]. This study conducted by Sun et al. [6] used a twin-camera high-speed imaging system to capture local deformations around the damaged area during the ultimate failure event of CFRP panels and compared the experimental results

with a numerical model. The study found good agreement between the experimental and numerical results, particularly with the formation of a local out-of-plane peak and trough surface profile around the damaged area caused by local buckling.

However, given the high cost of high-speed cameras, efforts have been made to reduce the cost of performing high-speed 3D DIC by means of designing single-camera imaging systems. A study conducted by López-Alba et al. [7] presented an imaging system that used four planar mirrors to reflect different angular views of a sample to each half of the camera field of view. The system was used for imaging of a quasi-static compression test as well as a dynamic drop-weight test and was validated in comparison with a conventional twin-camera 3D DIC system. The study concluded that the single-camera 3D DIC system had differences of less than 1% in displacement measurements and less than 5% in strain measurements when compared with its twin-camera counterpart. A study conducted by Pan et al. [8] incorporated a four-mirror optical system into a single-camera high-speed imaging system to measure 3D deformations in ballistic impact testing of aluminum and 3D braided CFRP panels. Results for the aluminum panel indicated that out-of-plane displacements measured by the single-camera system have excellent agreement with direct measurements using a Vernier caliper. Results for the CFRP panel allowed for the identification of various damage mechanisms that occurred during the test, including swelling and delamination. The four-mirror optical system, when applied to high-speed imaging, can therefore be used for full-field 3D deformation and strain measurement at a significantly reduced cost.

In this work, the fracture event of large CFRP panels during compression after impact testing is examined using a single-camera high-speed 3D DIC system with an optical configuration of four planar mirrors. This work focuses specifically on the findings for the panel impacted with 75 Joule (J) of impact energy to demonstrate the imaging system and the visualization of 3D DIC results. The objective of this work is to demonstrate the effectiveness of the single-camera system through the investigation of fracture mechanisms of CFRP panels under compressive loading, using out-of-plane displacement and strain fields to identify the stages of the fracture event.

2 Methods

2.1 Sample Preparation

2.1.1 Sample Manufacturing

The CFRP laminate panels used in this study were manufactured from IM7/977-3 Carbon/Epoxy prepreg in an autoclave, following the recommended temperature and pressure cure cycle by the material supplier (Cytec Engineered Materials, CA, USA). The test panels were then inspected using ultrasound and machined to the final dimensions by waterjet. The final dimensions of 254 mm x 304.8 mm x 4.3 mm (10” x 12” x 0.171”) are shown in Figure 1(a). The panels had a quasi-isotropic layup configuration of $[0/45/90/-45]_{4s}$. A total of 4 panels were tested using high-speed imaging.

2.1.2 Drop-Weight Impact Testing

The panels were subjected to drop-weight impact testing using a drop-weight system (Dynatup 8200, Instron, Norwood, MA), based on a modified version of the ASTM D7136/D7136M standard [9]. A hemispherical tip impactor with a diameter of 25.4 mm (1”) was used to impact a given sample at the designated impact energy level of 75J.

2.1.3 Surface Preparation and Painting

Surface preparation and painting were done to ensure effective DIC measurement. The panels were first cleaned throughout using ethanol to remove contaminants from the surfaces, thereby ensuring good uniformity and adhesion when applying a coat of paint. Next, a flat black base coat (Flat Black Spray Paint, Rust-Oleum, Concord, Ontario, Canada) was applied to the front and back surfaces, such that the surfaces had low reflectance for imaging.

A speckling pattern of paint (Opaque White 5212, Createx Colors, East Granby, CT) was then applied to the front and back surfaces of the test panels, using an airbrush (H-SET, Paasche Airbrush Company, Chicago, IL). The pseudo-random pattern was achieved using a technique involving spraying the paint onto a disposable flat surface directed at the panels (i.e., a wooden tongue depressor), allowing large droplets of paint to form at the edges before they are sprayed onto the panels, creating a coarse stippling effect. The panel after preparation is shown in Figure 1. Figure 1(a) shows a CAD model of a panel with an illustrative speckle pattern texture applied to the surface. Figure 1(b) shows a physical example of a panel with a painted speckle pattern applied to the surface. Figure 1(c) shows the painted speckle pattern in an amplified view.

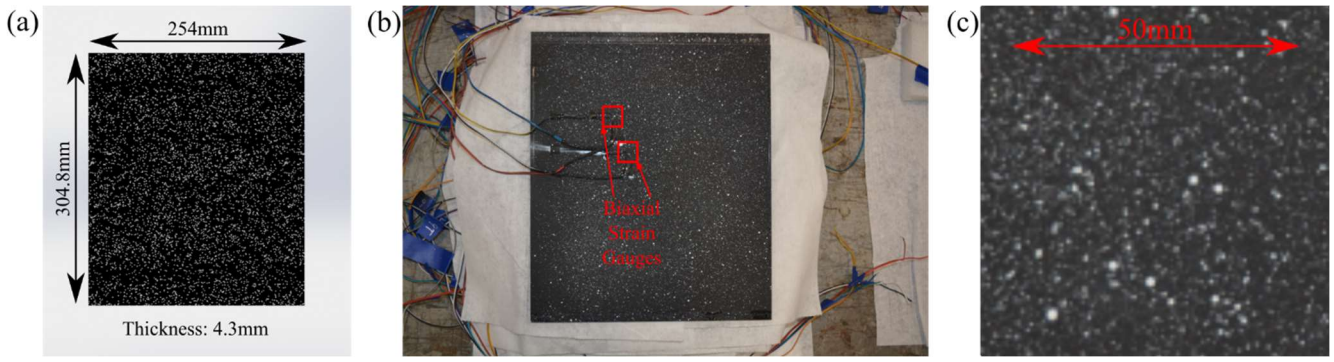

Figure 1: CFRP test panel: (a) schematic with dimensions and illustrative speckle pattern; (b) panel with mounted biaxial strain gauges; (c) amplified speckle pattern.

2.2 High-Speed Imaging Setup

A high-speed camera (Phantom v1611, Vision Research, Wayne, NJ) and a four-mirror optical setup were used for high-speed stereo imaging of the front side of the sample. The camera used a variable focal length lens (AF Zoom-NIKKOR 24-85mm f/2.8-4D IF, Nikon, Tokyo, Japan) at a focal length of 85 mm and an aperture size of f/5.6. Images were acquired at a rate of 12,000 frames per second for up to 5.5 seconds per test. The samples were illuminated using two continuous video lights (SL-60W CRI95+, Godox, Shenzhen, China). The camera and image properties for the high-speed imaging system are listed in Table 1. The full image acquisition setup is shown in Figure 2.

Table 1: Properties of high-speed imaging setup.

Property	Unit	Value
Camera Resolution	$px \times px$	1280 x 800
Pixel Size	μm	28
Frame Rate	Hz	12,000
Image Scaling Factor	px/mm	3.0
Combined Virtual Field of View	$mm \times mm$	426.7 x 266.7
System Virtual Stereo Angle	° (deg)	19.9

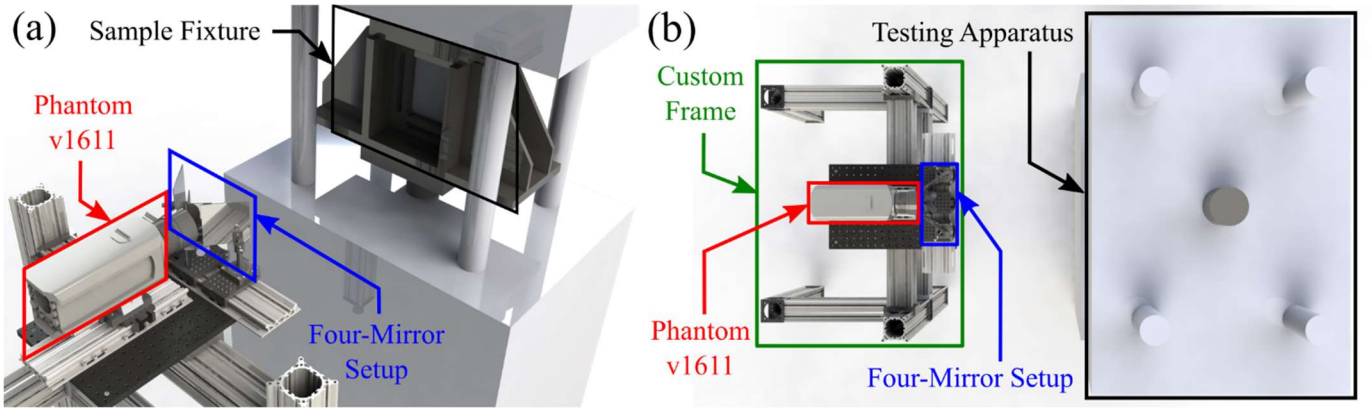

Figure 2: Full high-speed imaging and testing setup for CAI testing of CFRP panels: (a) isometric view of optomechanical hardware and sample fixture; (b) top view of custom structural frame and testing apparatus; (c) schematic of four-mirror configuration.

The optomechanical setup for the camera and mirrors, shown in Figure 2(a), was assembled on an optical breadboard (MB1218, Thorlabs, Newton, NJ), and includes rails, posts, and plate holders, to which the camera and mirrors were installed, allowing for adjustable spacing and orientation of hardware. The full imaging hardware, shown in Figure 2(b), consists of a custom structural frame comprised of 95 mm aluminum extrusions (X95 Extrusions, Thorlabs, Newton, NJ), connected using corner cubes (XT95C1, Thorlabs, Newton, NJ) for rigid connections, as well as sliding connections (XT95P13, Thorlabs, Newton, NJ), supporting the optical breadboard and allowing for adjustable camera height.

The optical setup for high-speed imaging is shown in Figure 3. The four-mirror configuration, using positions and orientations shown in Figure 3(a), uses two 50.8 mm x 101.6 mm (2” x 4”) planar mirrors to split the field of view into two halves and two 101.6 mm x 101.6 mm (4” x 4”) planar mirrors for reflection towards the sample on each half. The optical setup creates two virtual cameras, such that each has half of the horizontal resolution of the high-speed camera, as illustrated by the acquired image in Figure 3(b).

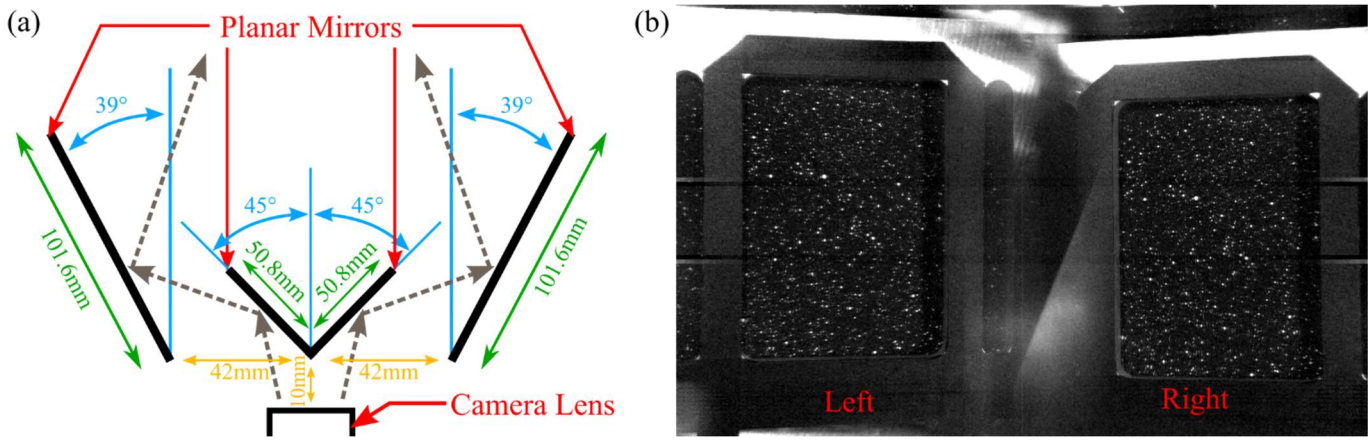

Figure 3: Optical setup for high-speed imaging: (a) schematic of four-mirror configuration; (b) image of the panel prior to fracture acquired by Phantom v1611, with contrast adjusted for clarity.

2.3 Compression After Impact Testing

Compression after impact testing was performed using a servohydraulic test system with a load capacity of 1 MN (220 kips) (Model 311.31, MTS, Eden Prairie, MN, USA). Each panel was subjected to boundary conditions involving anti-buckling guides based on a modified version of the ASTM D7137/D7137M standard [10] with added front and back support plates to reduce global buckling. The compression after impact fixture used in this study is shown in Figure 4. The added support plates, shown in Figure 4, limited the visible area to a central 127 mm x 177.8 mm (5" x 7") area.

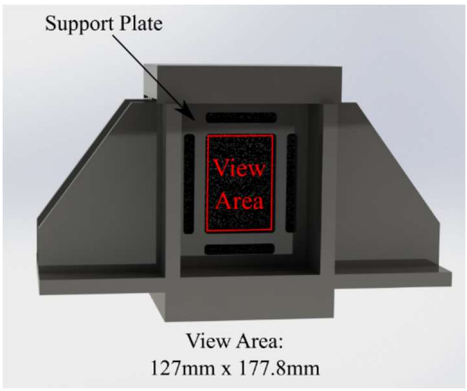

Figure 4: Compression After Impact fixture with added support plates.

2.4 Image Acquisition

Images of the fracture event were acquired using Phantom Camera Control and a manual button trigger (Pickle Switch, Vision Research, Wayne, NJ). The trigger was activated after the audible fracture event, allowing the camera to acquire a set of pre-trigger frames, within which the fracture event can be identified. The set of frames was saved as a CINE file, then converted to TIFF format using a software development kit for MATLAB (Phantom SDK Version 13.5.792.0, Vision Research, Wayne, NJ) that recognizes Phantom camera files.

2.5 Image Processing

For each test, 201 frames, particularly one identified reference frame near the fracture event and 100 frames both before and after this reference frame, were processed, generating measurements such that the start and development of the fracture event can be confidently identified. The frames were divided into two halves to create image pairs from the virtual cameras. Image pairs were processed, without pre-processing, using a commercial DIC software package (DaVis 10.0.3, LaVision GmbH, Göttingen, Germany), where 3D deformations and strains were evaluated at each frame. The imaging system was calibrated using a two-level 3D calibration plate (Type 204-15, LaVision GmbH, Göttingen, Germany). A correlation was performed for each frame relative to the first processed frame to prevent compounding precision errors. A subset size of 31 pixels and a step size of 10 pixels were used in the correlation procedure to preserve measurement accuracy amid image noise due to low camera exposure.

3 Results & Discussion

3.1 Out-of-Plane Displacement

The out-of-plane displacement results for the fracture event are shown in Figure 5. The values in Figure 5(a) were evaluated by averaging the out-of-plane displacement measurements over the full visible area at each frame. The fracture event start (i.e., t = 0 ms) was defined at the frame after which out-of-plane displacement magnitudes

increased significantly. The out-of-plane displacement profiles are shown in Figure 5(b) with four time intervals from the fracture event start. Within 0.08 ms, a crack initiated around the impact-damaged area near the centre of the panel and occupies about half of the visible width, caused by local buckling represented by a peak and trough deformation profile with maximum displacement magnitudes of about 0.5 mm at each panel half. Within 0.17 ms, the crack propagated across the fully visible width, and the panel halves began to separate. Within 0.25 ms, the top and bottom panel halves were separated by about 2 mm out-of-plane, the maximum value across all processed frames.

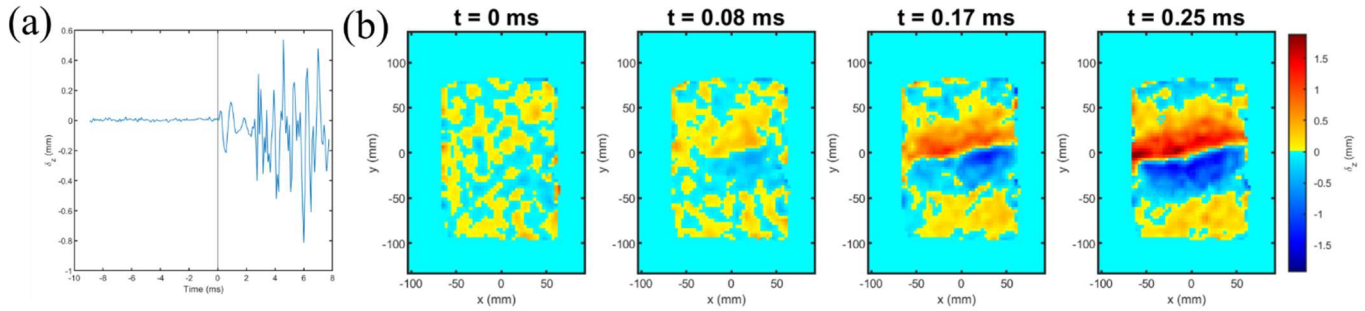

Figure 5: Out-of-plane displacement measurements: (a) averaged values vs time; (b) profiles. The vertical line at time t = 0 ms in (a) indicates the identified fracture event start.

3.2 Axial Strain

The axial strain results for the fracture event are shown in Figure 6. The values in Figure 6(a) were evaluated by averaging the axial strain measurements over the full visible area at each frame. The fracture event start coincided with the frame, after which average strain values began to drop significantly. The axial strain profiles are shown in Figure 6(b) with four time intervals from the fracture event start. Within 0.08 ms, a horizontal area around the damaged region, occupying about half of the visible width, experienced a compressive strain of about 1%, or 10,000 microstrain, corresponding to local buckling and crack initiation. Within 0.17 ms, a maximum compressive strain of about 1.2%, or 12,000 microstrain, was present across the fully visible width, corresponding to full crack propagation. In addition, the panel halves also experienced elastic recovery with maximum values of about 0.6%, or 6,000 microstrain.

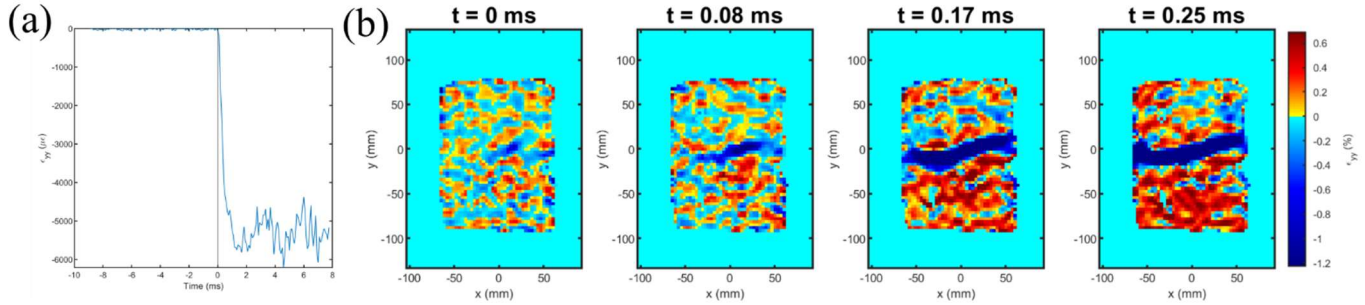

Figure 6: Axial strain measurements: (a) averaged values vs time; (b) profiles. The vertical line at time t = 0 ms in (a) indicates the identified fracture event start.

The study conducted by Sun et al. [6] estimated a fracture event duration for similar CFRP laminates, particularly those manufactured from IM7/8552 prepreg in a quasi-isotropic $[45/0/90/-45]_{4s}$ configuration, to be about 0.2 ms. The study also found a characteristic peak and trough deformation profile at the early stages of the fracture event. Although this work investigates laminates from IM7/977-3 prepreg in a $[0/45/90/-45]_{4s}$ configuration, the results from this work agree with the results found in the study by Sun et al. [6]. Estimation of fracture event duration can be made more precise by using higher frame rates, which would potentially require sample illumination of a higher power.

The study conducted by Pan et al. [8] used a camera with a resolution of 896 x 400 pixels and a frame rate of 21,000 frames per second, using a lens with a focal length of 50 mm and an aperture size of f/16, yielding a combined field of view of 246 mm x 110 mm. The correlation process in the study used a subset size of 31 pixels and a step size of 3 pixels, yielding thoroughly resolved deformation contours in an aluminum panel, as well as indicating local impact damage mechanisms in a CFRP panel. The results from the study provide a basis for further investigation in this work, particularly by examining the effects of subset step size and image pre-processing schemes to improve the deformation profile resolution without hindering measurement accuracy.

The single-camera high-speed imaging system is therefore effective in 3D DIC measurement for fracture analysis of CFRP panels in CAI testing, as the measurements have sufficient spatial and temporal resolutions to allow for identification of various stages of the fracture event, particularly the development and full propagation of local buckling. The imaging system in this work uses a high-speed camera that costs around $100,000 CAD, as well as structural and optomechanical components that cost around $8,000 CAD. As such, the full system costs around 54% of a corresponding conventional twin-camera high-speed imaging system, thus providing a significant cost benefit.

Conclusions

Compressive fracture properties were investigated in compression after impact testing of CFRP panels under boundary conditions with added support plates, where full-field optical measurement using single-camera high-speed 3D DIC at one face of the panel was demonstrated. A stereo view of the panel was achieved using a configuration of four planar mirrors that split the field of view into two parts and reflect a different angular view to each half. The acquired images were then fragmented to form image pairs. This work examined the case for a panel with 75J of impact energy and is part of a larger study that also examines other impact energy levels (no impact damage, 30J, and 30J three times). Out-of-plane displacement measurements demonstrated the development and full propagation of local buckling across the width of the panel during the failure event. Axial strain measurements demonstrated maximum compressive strain within the local buckling region and maximum strain relaxation caused by elastic recovery of the separated panel halves. The measured fracture behaviour of the panel agreed well with findings from previous work [6] from other labs, which indicate a similar deformation profile characterized by a peak at one panel half and a trough at the other, and a similar fracture event duration of about 0.2 ms. The single-camera high-speed imaging method can therefore be applied to assess the fracture behaviour of CFRP panels subjected to a range of impact energy levels and can provide a significant cost benefit over conventional twin-camera imaging methods.

References

[1] Q. Liang, J. Liu, X. Wang, X. Liu, D. Zhang, and K. Qian, “Flexural progressive failure mechanism of hybrid 3D woven composites: Combination of X-ray tomography, acoustic emission and digital image correlation,” *Composite Structures*, vol. 280, Jan. 2022, doi: 10.1016/J.COMPSTRUCT.2021.114894.

[2] Y. Wan, B. Yang, P. Jin, Z. Zheng, and Y. Huang, "Impact and compression-after-impact behavior of sandwich panel comprised of foam core and wire nets/glass fiber reinforced epoxy hybrid facesheets," *Journal of Sandwich Structures and Materials*, vol. 23, no. 6, pp. 2614–2637, Sep. 2021, doi: 10.1177/1099636220912785.

[3] K. Pan, R. C. Yu, G. Ruiz, X. Zhang, Z. Wu, and Á. de La Rosa, "The propagation speed of multiple dynamic cracks in fiber-reinforced cement-based composites measured using DIC," *Cement and Concrete Composites*, vol. 122, Sep. 2021, doi: 10.1016/j.cemconcomp.2021.104140.

[4] T. Lisle, C. Bouvet, N. Hongkarnjanakul, M. L. Pastor, S. Rivallant, and P. Margueres, "Measure of fracture toughness of compressive fiber failure in composite structures using infrared thermography," *Composites Science and Technology*, vol. 112, pp. 22–33, May 2015, doi: 10.1016/j.compscitech.2015.03.005.

[5] Y. Yuan and S. Wang, "Measurement of the energy release rate of compressive failure in composites by combining infrared thermography and digital image correlation," *Composites Part A: Applied Science and Manufacturing*, vol. 122, pp. 59–66, Jul. 2019, doi: 10.1016/j.compositesa.2019.04.022.

[6] X. C. Sun and S. R. Hallett, "Failure mechanisms and damage evolution of laminated composites under compression after impact (CAI): Experimental and numerical study," *Composites Part A: Applied Science and Manufacturing*, vol. 104, pp. 41–59, Jan. 2018, doi: 10.1016/j.compositesa.2017.10.026.

[7] E. López-Alba, L. Felipe-Sesé, S. Schmeer, and F. A. Díaz, "Optical low-cost and portable arrangement for full field 3D displacement measurement using a single camera," *Measurement Science and Technology*, vol. 27, no. 11, Sep. 2016, doi: 10.1088/0957-0233/27/11/115901.

[8] B. Pan, L. Yu, Y. Yang, W. Song, and L. Guo, "Full-field transient 3D deformation measurement of 3D braided composite panels during ballistic impact using single-camera high-speed stereo-digital image correlation," *Composite Structures*, vol. 157, pp. 25–32, Dec. 2016, doi: 10.1016/j.compstruct.2016.08.017.

[9] "ASTM D7136/D7136M-20 Standard Test Method for Measuring the Damage Resistance of a Fiber-Reinforced Polymer Matrix Composite to a Drop-Weight Impact Event," in *Annual Book of ASTM Standards*, vol. 15.03, 2020.

[10] "ASTM D7137/D7137M-17 Standard Test Method for Compressive Residual Strength Properties of Damaged Polymer Matrix Composite Plates," in *Annual Book of ASTM Standards*, vol. 15.03, 2017.